Supplementary Information

Chiral Co-assembled Exciplex Host Achieved Extremely Outstanding Narrowband Circularly Polarized Electroluminescence

Chao Liu, Jun Zeng, Zhenhao Jiang, Yihan Chen, Junsheng Zhang,* and Yixiang Cheng**

C. Liu, J. Zeng, Z. Jiang, J. Zhang, Y. Cheng

State Key Laboratory of Analytical Chemistry for Life Sciences, Engineering Research Center of Photoresist Materials, Ministry of Education, School of Chemistry and Chemical Engineering, Nanjing University. 163 Xianlin Avenue, Nanjing, 210023, P.R. China

E-mail: zhangjs@nju.edu.cn, yxcheng@nju.edu.cn

Y. Chen

School of Chemistry and Materials Science, Jiangsu Normal University, Xuzhou, 221116, P.R. China

E-mail: 6020240050@jsnu.edu.cn

Table of Contents

1. Experimental section.

Materials and methods. All NMR spectra were obtained by using a Bruker (400 MHz) spectrometer. Chemical shifts were recorded as parts per million (ppm, δ) relative to tetramethylsilane (δ 0.00) or chloroform (δ = 7.26, singlet). ^{1}H NMR splitting patterns are designated as singlet (s), doublet (d), triplet (t), multiplets (m) and etc. Ultraviolet-visible (UV-*vis*) spectra were measured by using a Shimadzu UV-3600 spectrophotometer. Fluorescence spectra was measured using Edinburgh FS5 and FLS 980 fluorescence spectrophotometer equipped with a xenon arc lamp (Xe 900), a nanosecond hydrogen flash-lamp (nF 920). The lifetimes were obtained on Edinburgh FLS 980. Thermo-gravimetry analysis (TGA) was performed on a NETZSCH STA 449 F3 Jupiter instrument in an atmosphere of N_2 at a heating rate of 10 ºC/min. The liquid crystalline textures were investigated and photographed using liquid crystal cells with a polarized optical microscope (POM) equipped with a Leitz 350 heating stage and an associated Nikon (D3100) digital camera. Differential scanning calorimetry (DSC) experiments were performed on a METTLER DSC 823e differential canning calorimeter at a scan rate of 10 ºC/min under the nitrogen atmosphere. Temperature-dependent, powder X-ray diffraction was measured on a small & wide-angle X-Ray scattering system (SAXSess mc^2, Cu-Kα, λ = 0.15418 nm). The absolute PL quantum yield were measured by Edinburgh FLS 980 with integrating sphere. Circular dichroism (CD) spectra were performed on a JASCO J-810 spectropolarimeter with 200 nm/min of scan speed. CPL spectra were collected on a JASCO CPL-300 spectrofluoropolarimeter. In the CPL measurements, scan speed was 100 nm/min, number of scans was 1, and slit width was 3000 μm. Scanning electron microscope (SEM) images were taken in Hitachi S-4800 field emission scanning electron microscopy. Chemicals and reagents were purchased from Aladdin, Alfa Aesar, Energy Chemical, Adamas-beta® and used as received without further purification. CzBN were synthesized according to previously reported literature.[S1]

Thermal Annealing Treatments. The thin film was prepared by dissolving the corresponding sample in toluene (20 mg mL^{-1}), followed by a spin coating (1000 rpm, 30 s) onto the quartz plate. The above quartz plates were put on the hot stage at 125 ºC

and the films were kept at this temperature for 20 min. Finally, the quartz plates were moved to room temperature. Device Fabrication and Characterization. The solution-processed multilayer OLEDs were fabricated as follows: Indium tin oxide (ITO)-coated glass substrates (1.5 cm × 1.5 cm) were cleaned with deionized water, and then sequentially ultrasonicated in dichloromethane (DCM), acetone and ethanol for 20 min, respectively. After finishing the preparatory work, the ITO substrates were treated in a UV-ozone oven for 20 min. Next, the 25 nm thickness PEDOT:PSS was spin-coated on the ITO substrates as the hole injection layer and dried at 120 ºC for 30 min to remove the solvent. After that, the emitting layer was spin-coated onto the PEDOT:PSS coated substrates and dried at 140 ºC for 30 min under N_2 atmosphere. Subsequently, 1,3,5-tris(N phenylbenz-imidazol-2-yl)-benzene (TPBi, 35 nm) was deposited by vacuum deposition as the electron transporting layer and hole blocking layer. Finally, Ca (10 nm) and Ag (100 nm) were sequentially deposited under 5 × 10^{-5} Pa pressure as the electron injection layer and cathode, respectively. The current-voltage, device brightness and electroluminescence spectra characteristics of OLEDs were detected by using the Keithley 2636A and Photo Research PR-655 Spectra Scan.

Electrochemical tests. CV measurements were performed on a CHI660D (Shanghai CH Instrument Company, China). Cyclic voltammograms of corresponding samples were measured in degassed DCM solution (1.0 × 10^{-3} mol/L) with 0.1 mol/L tetrabutylammonium hexafluorophosphate (Bu_4NPF_6 was purified by recrystallization in EtOH before being used) as the supporting electrolyte with a scan rate of 100 mV/s. Potentials are reported vs the Fc/Fc+ redox couple as an external reference. Counter electrode: Pt wire, working electrode: glassy carbon, and reference electrode: Ag/AgCl, with KCl (3 mol/L in deionized water) as a filling solution.

Computational Details: Computational studies were carried out using Gaussian 09 program package.[S2] The molecular orbitals distribution was investigated at B3LYP-D3/6-31G* level.[S3]

2. Synthesis and characterizations

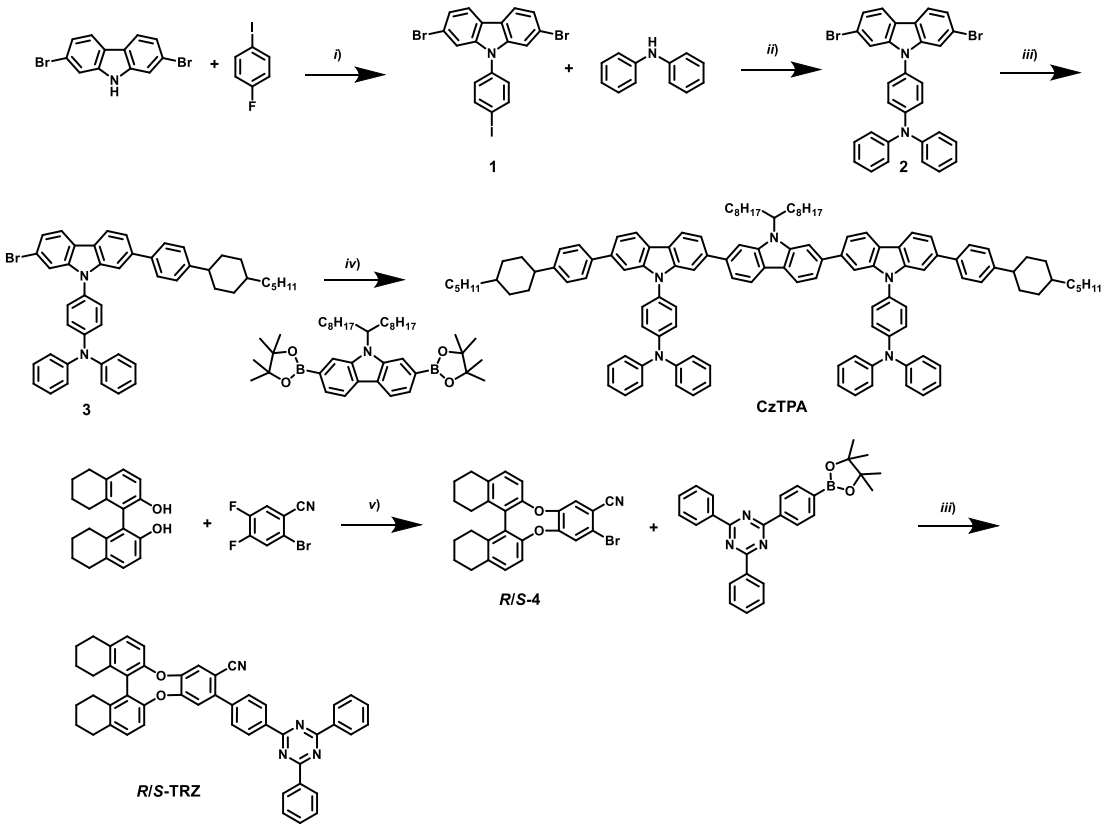

Synthesis of copolymers CzTPA: Reagents and conditions: (*i*) K_2CO_3, DMF, 150 °C, 24 h, 76%; (*ii*) $Pd_2(dba)_3$, t-BuOK, tri-tert-butylphosphine tetrafluoroborate, 90 °C, 12 h, 70%; (*iii*) K_2CO_3, $Pd(PPh_3)_4$, toluene/H_2O, 85 °C, 12 h, 42%; (*iv*) K_2CO_3, $Pd(PPh_3)_4$, toluene/EtOH/H_2O, 85 °C, 12 h, 89%; (*v*) K_2CO_3, DMF, 120 °C, 12 h, 88%

a) Synthesis and characterizations of 1.

Compound 1 were synthesized according to the literature.[S4]

^{1}H NMR (400 MHz, Chloroform-*d*) δ 7.99 – 7.91 (m, 4H), 7.46 (d, *J* = 1.6 Hz, 2H), 7.41 (dd, *J* = 8.3, 1.7 Hz, 2H), 7.26 (d, *J* = 8.6 Hz, 2H).

b) Synthesis and characterizations of 2.

Compounds 1 (1.0 equiv, 0.7 g), diphenylamine (1.0 equiv, 782 mg), t-BuOK (2.5 equiv, 1.16 g), $Pd_2(dba)_3$ (0.03 equiv, 114 mg) and tri-tert-butylphosphine tetrafluoroborate (0.05 equiv, 60 mg) were dissolved in 30 mL dry toluene under Ar atmosphere. After the mixture was stirred at 85 ℃ for 12 h. The reaction mixture was added H_2O (30 ml) and extracted with CH_2Cl_2 (3 × 30 ml). The organic layer was washed with saturated NaCl solution and dried over anhydrous sodium sulfate. The

precipitate was removed by filtration, and filtrate was evaporated under reduced pressure. The residue was purified by column chromatography (eluent: petroleum ether/DCM = 10/1) to give compound 2 (1.65 g, 70%) as a white solid.

^{1}H NMR (400 MHz, Chloroform-*d*) δ 7.90 (d, *J* = 8.3 Hz, 2H), 7.50 (d, *J* = 1.6 Hz, 2H), 7.39 – 7.31 (m, 6H), 7.28 – 7.21 (m, 8H), 7.14 – 7.08 (m, 2H). ^{13}C NMR (101 MHz, Chloroform-*d*) δ 148.03, 147.29, 142.17, 129.60, 129.46, 127.83, 125.19, 123.82, 123.46, 123.43, 121.54, 121.44, 119.93, 113.12.

c) Synthesis and characterizations of 3.

Compounds 2 (1.0 equiv, 1.62 g), 4-(trans-4-pentylcyclohexyl)phenylboronic acid (1.0 equiv, 782 mg), K_2CO_3 (4.0 equiv, 1.58 g), $Pd(PPh_3)_4$ (0.03 equiv, 99 mg) were dissolved in 30 mL toluene/H_2O (*v*/*v* = 5/1) under Ar atmosphere. After the mixture was stirred at 85 ℃ for 12 h. The reaction mixture was added H_2O (30 ml) and extracted with CH_2Cl_2 (3 × 30 ml). The organic layer was washed with saturated NaCl solution and dried over anhydrous sodium sulfate. The precipitate was removed by filtration, and filtrate was evaporated under reduced pressure. The residue was purified by column chromatography (eluent: petroleum ether/DCM = 5/1) to give compound 3 (859 mg, 42%) as a white solid.

^{1}H NMR (400 MHz, Chloroform-*d*) δ 8.09 (d, *J* = 8.1 Hz, 1H), 7.95 (d, *J* = 8.3 Hz, 1H), 7.55 (d, *J* = 8.1 Hz, 2H), 7.54 – 7.51 (m, 2H), 7.49 (dd, *J* = 8.1, 1.5 Hz, 1H), 7.37 (dd, *J* = 8.2, 1.7 Hz, 1H), 7.35 – 7.30 (m, 6H), 7.28 (d, *J* = 7.9 Hz, 3H), 7.25 – 7.20 (m, 6H), 7.09 (t, *J* = 7.3 Hz, 2H), 2.51 (tt, *J* = 12.2, 3.2 Hz, 1H), 1.95 – 1.85 (m, 4H), 1.53 – 1.42 (m, 2H), 1.34 – 1.21 (m, 9H), 1.06 (dt, *J* = 13.1, 10.2 Hz, 2H), 0.90 (t, *J* = 6.9 Hz, 3H). ^{13}C NMR (101 MHz, Chloroform-*d*) δ 147.64, 147.39, 147.09, 142.45, 141.96, 140.02, 139.46, 130.26, 129.54, 127.93, 127.53, 127.27, 125.08, 123.66, 123.59, 123.02, 122.02, 121.58, 121.39, 120.43, 119.97, 119.40, 112.87, 108.46, 44.35, 37.43, 37.36, 34.42, 33.65, 32.26, 26.70, 22.77, 14.17.

d) Synthesis and characterizations of CzTPA.

Compounds 3 (2.5 equiv, 327 mg), 9-(9-heptadecanyl)-9H-carbazole-2,7-diboronic acid bis(pinacol) ester (1.0 equiv, 120 mg), K_2CO_3 (8.0 equiv, 202 mg), $Pd(PPh_3)_4$ (0.05 equiv, 11 mg) were dissolved in 14 mL toluene/EtOH/H_2O (*v*/*v*/*v* = 5/1/1) under Ar

atmosphere. After the mixture was stirred at 85 ℃ for 12 h. The reaction mixture was added H_2O (20 ml) and extracted with CH_2Cl_2 (3 × 20 ml). The organic layer was washed with saturated NaCl solution and dried over anhydrous sodium sulfate. The precipitate was removed by filtration, and filtrate was evaporated under reduced pressure. The residue was purified by column chromatography (eluent: petroleum ether/DCM = 2 : 1) to give compound CzTPA (273 mg, 89%) as a white solid.

^{1}H NMR (400 MHz, Chloroform-*d*) δ 8.20 (td, *J* = 10.5, 9.4, 6.1 Hz, 6H), 7.84 (s, 1H), 7.72 (s, 2H), 7.66 (d, *J* = 5.9 Hz, 2H), 7.61 (d, *J* = 7.8 Hz, 6H), 7.56 – 7.51 (m, 4H), 7.48 (d, *J* = 8.6 Hz, 4H), 7.32 (t, *J* = 8.1 Hz, 16H), 7.25 – 7.19 (m, 9H), 7.08 (t, *J* = 7.4 Hz, 4H), 4.70 (dt, *J* = 10.3, 5.2 Hz, 1H), 2.53 (tt, *J* = 12.0, 3.3 Hz, 2H), 2.40 (dtd, *J* = 14.5, 9.8, 4.5 Hz, 2H), 1.94 (dtd, *J* = 18.0, 14.3, 13.2, 6.9 Hz, 11H), 1.55 – 1.45 (m, 5H), 1.34 – 1.21 (m, 24H), 1.15 – 1.06 (m, 22H), 0.91 (t, *J* = 6.9 Hz, 6H), 0.75 (t, *J* = 6.9 Hz, 6H). ^{13}C NMR (101 MHz, Chloroform-*d*) δ 147.51, 147.30, 146.95, 143.11, 142.27, 140.71, 140.65, 140.06, 139.70, 139.51, 131.14, 129.50, 128.07, 127.55, 127.26, 124.96, 123.80, 123.51, 122.87, 122.18, 122.13, 121.50, 120.46, 120.19, 119.68, 119.04, 110.65, 108.91, 108.34, 107.98, 56.46, 44.37, 37.45, 37.38, 34.44, 33.89, 33.68, 32.27, 31.77, 29.50, 29.37, 29.17, 26.88, 26.71, 22.77, 22.59, 14.18, 14.06.

e) Synthesis and characterizations of *R*/*S*-4.

Compound *R*/*S*-4 were synthesized according to the literature.[S5]

^{1}H NMR (400 MHz, Chloroform-*d*) δ 7.48 (s, 1H), 7.46 (s, 1H), 7.10 (dd, *J* = 8.3, 3.0 Hz, 2H), 6.92 (dd, *J* = 8.2, 6.3 Hz, 2H), 2.83 (q, *J* = 9.5, 7.9 Hz, 4H), 2.64 (ddd, *J* = 16.2, 8.0, 3.9 Hz, 2H), 2.41 – 2.33 (m, 2H), 1.84 – 1.75 (m, 6H), 1.65 (tt, *J* = 8.5, 4.5 Hz, 2H).

f) Synthesis and characterizations of *R*-TRZ.

Compounds *R*-4 (1.0 equiv, 450 mg), 2,4-diphenyl-6-(4-(4,4,5,5-tetramethyl-1,3,2-dioxaborolan-2-yl)phenyl)-1,3,5-triazine (1.0 equiv, 415 mg), K_2CO_3 (4.0 equiv, 527 mg), $Pd(PPh_3)_4$ (0.05 equiv, 55 mg) were dissolved in 24 mL toluene/H_2O (*v*/*v*/*v* = 5/1/1) under Ar atmosphere. After the mixture was stirred at 85 ℃ for 12 h. The reaction mixture was added H_2O (20 ml) and extracted with CH_2Cl_2 (3 × 25 ml). The organic layer was washed with saturated NaCl solution and dried over anhydrous sodium sulfate.

The precipitate was removed by filtration, and filtrate was evaporated under reduced pressure. The residue was purified by column chromatography (eluent: petroleum ether/DCM = 1/1) to give compound *R*-TRZ (587 mg, 88%) as a white solid.

g) Synthesis and characterizations of *S*-TRZ.

S-TRZ was synthesized in the same way of preparing *R*-TRZ, just replaced *R*-4 with equivalent stoichiometric *S*-4.

^{1}H NMR (400 MHz, Chloroform-*d*) δ 8.92 – 8.86 (m, 2H), 8.85 – 8.75 (m, 4H), 7.76 (d, *J* = 8.2 Hz, 2H), 7.68 (d, *J* = 1.8 Hz, 1H), 7.60 (tdd, *J* = 8.6, 6.3, 4.0 Hz, 6H), 7.44 (d, *J* = 1.3 Hz, 1H), 7.16 (t, *J* = 7.7 Hz, 2H), 7.04 (ddd, *J* = 8.0, 6.3, 1.4 Hz, 2H), 2.87 (dq, *J* = 16.7, 10.5, 8.3 Hz, 4H), 2.72 (ddt, *J* = 16.6, 8.7, 4.4 Hz, 2H), 2.46 (dq, *J* = 16.7, 5.7 Hz, 2H), 1.87 (p, *J* = 6.4 Hz, 6H), 1.79 – 1.64 (m, 2H). ^{13}C NMR (101 MHz, Chloroform-*d*) δ 171.69, 171.03, 153.37, 150.54, 150.39, 149.21, 141.61, 141.01, 137.04, 136.97, 136.59, 136.14, 135.77, 135.63, 132.60, 130.29, 130.21, 129.99, 129.89, 129.42, 129.03, 128.95, 128.67, 128.13, 124.29, 118.53, 118.49, 117.99, 106.41, 29.42, 27.72, 27.67, 22.80, 22.68.

3. TGA and DSC curves.

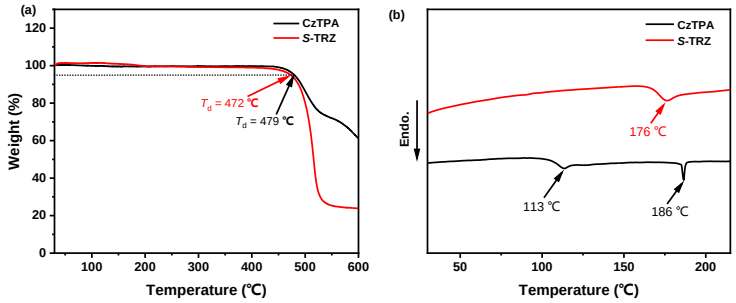

Fig. S1. (a) TGA and (b) DSC curves of CzTPA and *S*-TRZ.

4. POM images.

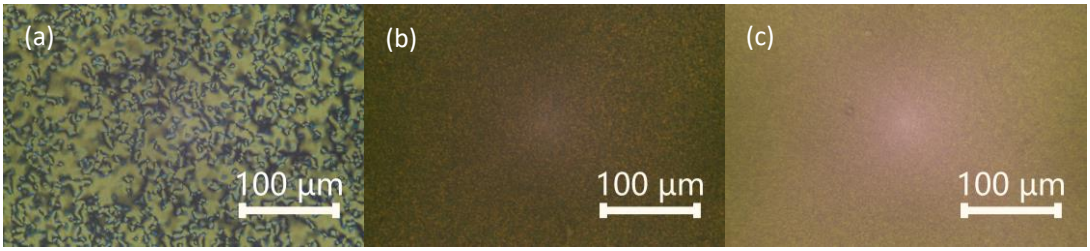

Fig. S2. POM images of (a) CzTPA (125 °C), (b) $(CzTPA)_{0.92}$-$(S\text{-}TRZ)_{0.08}$ (125 °C), (c) $(CzTPA)_{0.92}$-$(S\text{-}TRZ)_{0.08}$-$(CzBN)_{0.003}$ (125 °C).

5. SAXS profiles.

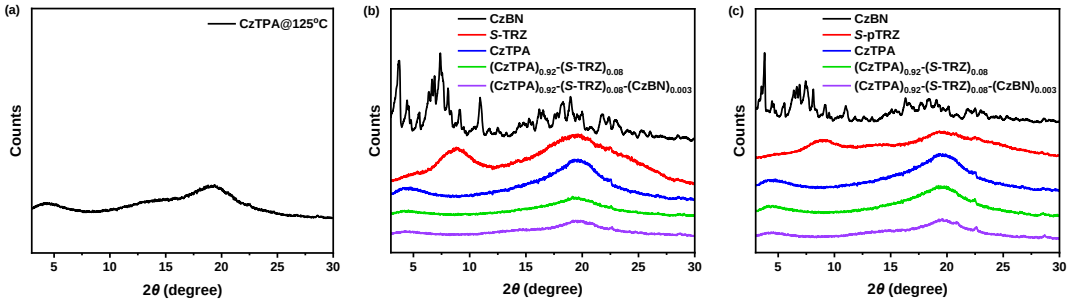

Fig. S3. The SAXS profiles of (a) CzTPA (125 °C); CzBN, *S*-TRZ, CzTPA, $(CzTPA)_{0.92}$-$(S\text{-}TRZ)_{0.08}$, and $(CzTPA)_{0.92}$-$(S\text{-}TRZ)_{0.08}$-$(CzBN)_{0.003}$ (b) before and (c) after thermal annealing at 125 °C.

6. Electrochemical measurement.

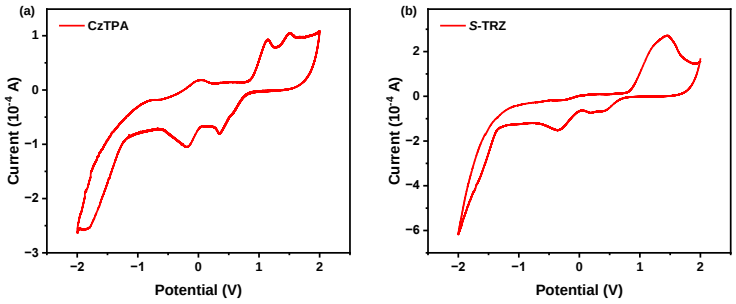

Fig. S4. CV curve of (a) CzTPA and (b) *S*-TRZ in CH_2Cl_2 solution.

Table S1. Electrochemical property of CzTPA and *S-TRZ*.

Compound	λ_{onset} (nm)	E_g[a] (eV)	$E_{ox,\ onset}$ (V)	HOMO/LUMO[a] (eV)	HOMO/LUMO[b] (eV)
CzTPA	323	3.84	0.70	-4.97/-1.13	-4.99/-1.20
S-TRZ	294	4.22	1.92	-6.19/-1.97	-6.23/-1.97

[a]Measured in CH_2Cl_2 at room temperature with ferrocene as an internal standard. [b]Obtained from theoretical calculations. $E_g = 1240/\lambda_{onset}$. $E_{HOMO} = -(E_{ox} - E_{(Fc/Fc+)} + 4.8)$ eV, $E_{(Fc/Fc+)} = 0.53$ V vs Ag/AgCl. $E_{LUMO} = E_{HOMO} + E_g$.

7. Photophysical Properties.

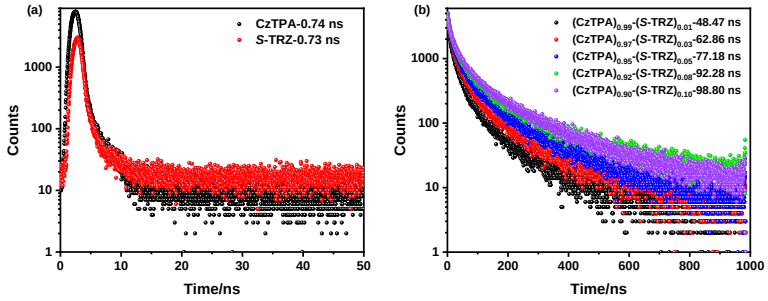

Fig. S5. The lifetime decay profiles of (a) CzTPA and *S*-TRZ; (b) $(CzTPA)_x$-$(S\text{-}TRZ)_y$ after thermal annealing at 125 °C (λ_{exc} = 320 nm).

Table S2. Optical properties of films CzTPA, *S*-TRZ and $(CzTPA)_x$-$(S\text{-}TRZ)_y$ after annealing at 125 °C

co-assembled films	FL (nm)	Φ_{PL} (%)	τ (ns)
CzTPA	442	59.08	0.74
S-TRZ	393	0.01	0.73
$(CzTPA)_{0.99}$-$(S\text{-}TRZ)_{0.01}$	445	35.11	48.47
$(CzTPA)_{0.97}$-$(S\text{-}TRZ)_{0.03}$	446	35.79	62.86
$(CzTPA)_{0.95}$-$(S\text{-}TRZ)_{0.05}$	482	35.60	77.18
$(CzTPA)_{0.92}$-$(S\text{-}TRZ)_{0.08}$	488	34.47	92.28
$(CzTPA)_{0.90}$-$(S\text{-}TRZ)_{0.10}$	493	33.15	98.80

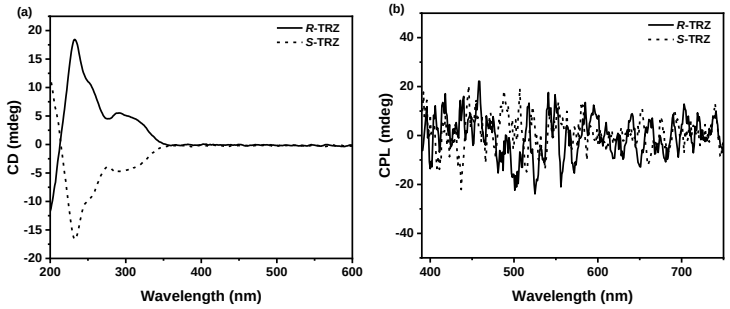

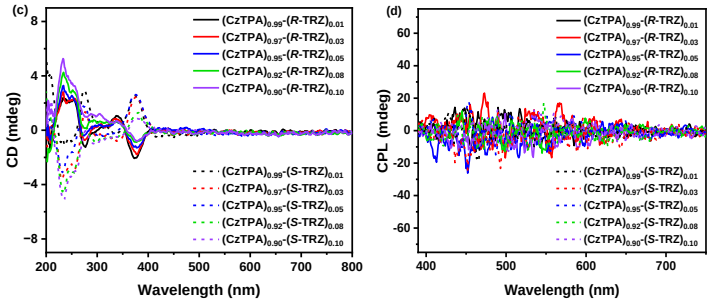

Fig. S6. (a) (c) CD and (b) (d) CPL spectra of *R*/*S*-TRZ, $(CzTPA)_x$-$(R/S\text{-}TRZ)_y$ in spin-coated films before annealing (λ_{exc} = 320 nm).

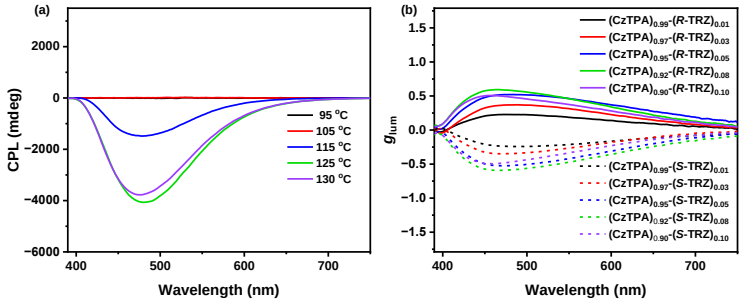

Fig. S7. (a) CPL spectra of $(CzTPA)_{0.92}$-$(S\text{-}TRZ)_{0.08}$ in spin-coated films at different annealing temperature; (b) The g_{lum} value curves of $(CzTPA)_x$-$(R/S\text{-}TRZ)_y$ in spin-coated films after annealing at 125 °C (λ_{exc} = 320 nm)

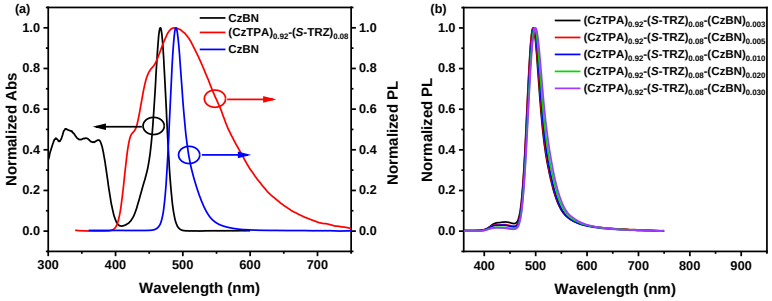

Fig. S8. (a) The normalized the absorption and PL spectra of CzBN and PL spectra of $(CzTPA)_{0.92}$-$(S\text{-}TRZ)_{0.08}$; (b) The normalized PL spectra of $(CzTPA)_{0.92}$-$(S\text{-}TRZ)_{0.08}$-$(CzBN)_z$.

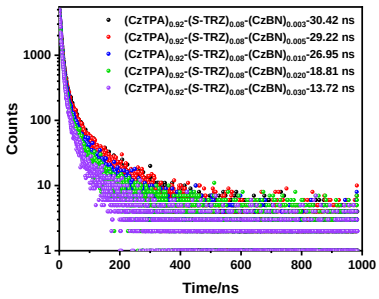

Fig. S9. The lifetime decay profiles of $(CzTPA)_{0.92}$-$(S\text{-}TRZ)_{0.08}$-$(CzBN)_z$ after thermal annealing at 125 °C (λ_{exc} = 320 nm).

Table S3. Optical properties of co-assembled films $(CzTPA)_{0.92}$-$(S\text{-}TRZ)_{0.08}$-$(CzBN)_z$ after annealing at 125 °C.

co-assembled film	FL (nm)	FWHM (nm)	Φ_{PL} (%)	τ (ns)
$(CzTPA)_{0.92}$-$(S\text{-}TRZ)_{0.08}$	488	139	34.47	92.28
$(CzTPA)_{0.92}$-$(S\text{-}TRZ)_{0.08}$-$(CzBN)_{0.003}$	495	33	68.82	30.42
$(CzTPA)_{0.92}$-$(S\text{-}TRZ)_{0.08}$-$(CzBN)_{0.005}$	496	33	68.10	29.22
$(CzTPA)_{0.92}$-$(S\text{-}TRZ)_{0.08}$-$(CzBN)_{0.010}$	497	34	67.49	26.95
$(CzTPA)_{0.92}$-$(S\text{-}TRZ)_{0.08}$-$(CzBN)_{0.020}$	498	35	64.20	18.81
$(CzTPA)_{0.92}$-$(S\text{-}TRZ)_{0.08}$-$(CzBN)_{0.030}$	500	37	57.18	13.72

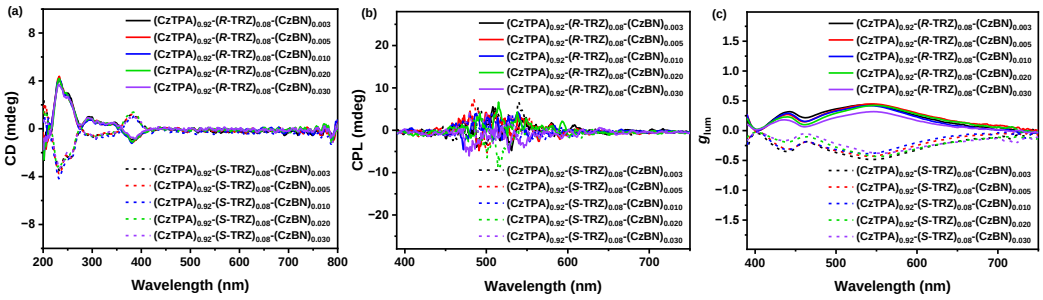

Fig. S10. (a) CD and (b) CPL spectra of $(CzTPA)_{0.92}$-$(R/S\text{-}TRZ)_{0.08}$-$(CzBN)_z$ in spin-coated films before annealing; (c) g_{lum} value curves of $(CzTPA)_{0.92}$-$(R/S\text{-}TRZ)_{0.08}$-$(CzBN)_z$ in spin-coated films

after annealing at 125 ℃. (λ_{exc} = 320 nm)

8. SEM images.

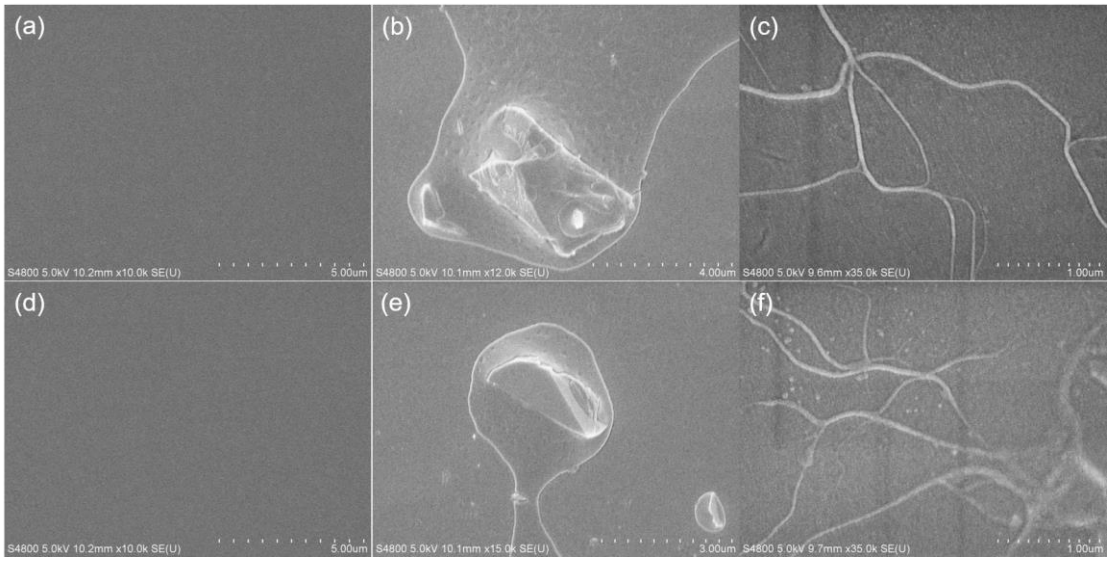

Fig. S11. SEM images of (a, b, c) $(CzTPA)_{0.92}$-$(S\text{-}TRZ)_{0.08}$ and (d, e, f) $(CzTPA)_{0.92}$-$(S\text{-}TRZ)_{0.08}$-$(CzBN)_{0.003}$. (a, d (spin-coated film, 20 mg/mL), b, e (film, 2×10^{-1} mg/mL), c, f (aggregate state, THF/H_2O = 60/40, v/v, 2×10^{-3} mg/mL), before thermal annealing).

9. AFM images.

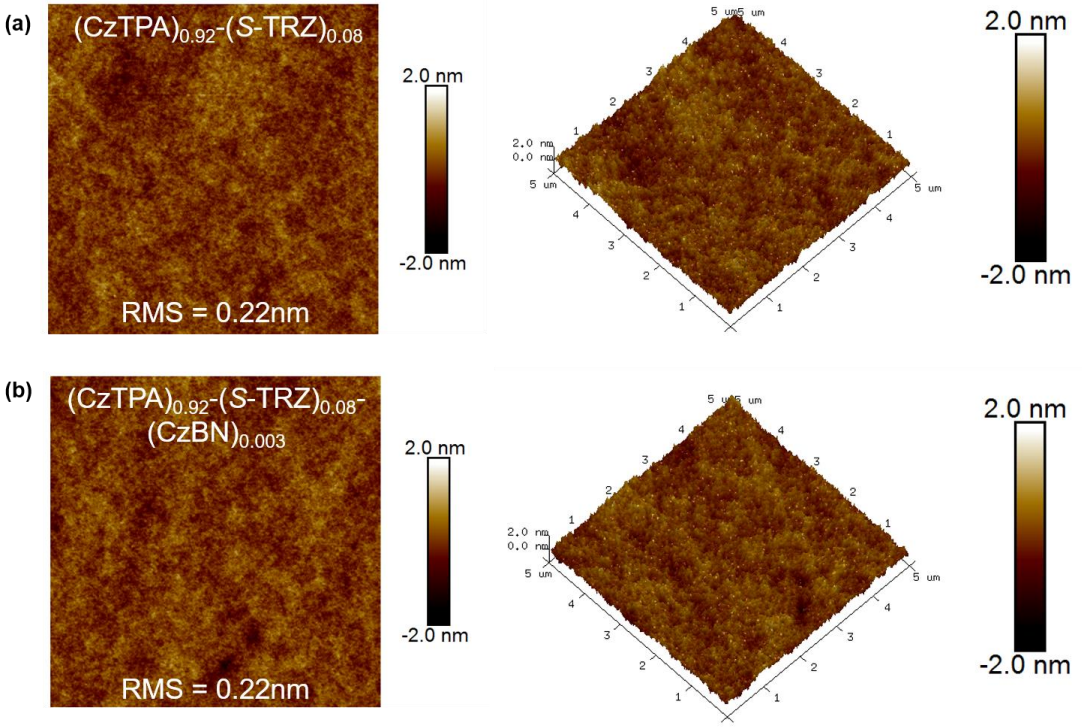

Fig. S12. (a) AFM images of (a) $(CzTPA)_{0.92}$-$(S\text{-}TRZ)_{0.08}$ and (b) $(CzTPA)_{0.92}$-$(S\text{-}TRZ)_{0.08}$-

$(CzBN)_{0.003}$.

10. EL performance of OLEDs.

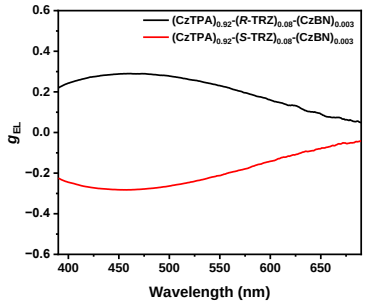

Fig. S13. g_{EL} curves of the devices based on $(CzTPA)_{0.92}$-(*R*/*S*-TRZ)$_{0.08}$-$(CzBN)_{0.003}$.

Table S4. Key device performance of CP-OLEDs

Device	λ_{EL} (nm)	FWHM (nm)	V_{on} (V)	L_{max} (cd m^{-2})	$CE_{max/100/1000}$ (cd A^{-1})	$EQE_{max/100/1000}$ (%)	g_{EL}	CIE(x, y)
R-D	488	33	7.5	4376	2.1/2.1/1.7	1.2/1.2/1.0	+0.28	(0.13, 0.38)
S-D	488	33	6.6	6471	3.4/3.4/2.9	2.0/2.0/1.7	-0.27	(0.13, 0.38)

Table S5. The g_{EL} values, EQE_{max}, and FWHM of reported CP-OLEDs (FWHM ≤ 50 nm).

Compounds	g_{EL}	**EQE_{max} (%)**	**FWHM (nm)**	**Reference**
$(CzTPA)_{0.92}$-(*R*-TRZ)$_{0.08}$-$(CzBN)_{0.003}$	**0.28**	**1.2**	**33**	**This work**
$(CzTPA)_{0.92}$-(*S*-TRZ)$_{0.08}$-$(CzBN)_{0.003}$	**-0.27**	**2.0**	**33**	
IBN9H	2.7×10^{-3}	33.5	26	*Adv. Opt. Mater.* **2025**, e02776
(*R*/*S*)-TQ-TPA	$4.7\text{-}5.8 \times 10^{-4}$	14.8	43	*Chem. Eng. J.* **2025**, *525*, 170368
$(2PFP)_{0.9}$-(*P*-THH)$_{0.1}$-$(BCz\text{-}BN)_{0.05}$	0.61	9.0	32	*Angew. Chem. Int. Ed.* **2025,** e202517906
$(2PFP)_{0.9}$-(*M*-THH)$_{0.1}$-$(BCz\text{-}BN)_{0.05}$	-0.60	8.9	32	
P/*M*-BN8H	7.1×10^{-4}	30.0	37	*Adv. Funct. Mater.* **2025**, e17999
(*P*)-DBN-mICz	5.3×10^{-3}	37.3	27	*Adv. Mater.* **2025**, e11560
(*M*)-DBN-mICz	-8.5×10^{-3}	36.6	27	
(*S*)-OBN-CO-NB	-2.2×10^{-3}	17.5	35	*Org. Lett.* **2025**, *27*, 10192
(*R*)-OBN-CO-NB	1.7×10^{-3}	17.7	35	

R-PCP-DBNO	1.2×10^{-3}	29.4	31	*Adv. Mater.* **2025**, e11230
S-PCP-DBNO	-1.1×10^{-3}	29.0	31	
BN-Tol	-	25.8	28	*Angew. Chem. Int. Ed.* **2025**, *64*, e202504057
BN-TPA	1.95×10^{-3}	28.5	28	
BN-PhCz	6.23×10^{-3}	30.4	28	
BN-DPXZ	6.53×10^{-3}	28.9	32	
5%(*M*)-ABH-BNCz	3.4×10^{-3}	30.8	26	*Adv. Mater.* **2025**, 2420611
5%(*P*)-ABH-BNCz	-3.3×10^{-3}	31.0	27	
10%(*M*)-ABH-BNCz	8.7×10^{-3}	33.5	30	
10%(*P*)-ABH-BNCz	-9.1×10^{-3}	32.4	30	
20%(*M*)-ABH-BNCz	16×10^{-3}	23.2	42	
20%(*P*)-ABH-BNCz	-18×10^{-3}	22.9	43	
R-m-ICz-N-BN	1.89×10^{-3}	33.7	26	*Adv. Funct. Mater.* **2025**, *35*, 2504525.
R-m-prCz-N-BN	1.88×10^{-3}	32.4	27	
R-DWBN	-1.5×10^{-3}	27.8	30	*Sci. China Chem.* **2025**. DOI:10.1007/s11426-025-2716-6
S-DWBN	1.0×10^{-3}	27.3	30	
(*R*)-BIPNX-BN	1.0×10^{-3}	24.2	27	*Chem. Eng. J.* **2025**, *505,* 159719
(*S*)-BIPNX-BN	-1.3×10^{-3}	-	-	
(*R*)-8H-BIPNX-BN	1.3×10^{-3}	23.4	30	
(*S*)-8H-BIPNX-BN	-1.9×10^{-3}	-	-	
(*R*)-8H-BIPTZ-BN	1.0×10^{-3}	26.3	28	
(*S*)-8H-BIPTZ-BN	-0.8×10^{-3}	-	-	
(R_{mt})-2	-2.0×10^{-3}	15.6	36	*Angew. Chem. Int. Ed.* **2025**, *64*, e202417458
(S_{mt})-2	2.1×10^{-3}	17.6	36	
(*R*)-S-AX-BN	3.3×10^{-3}	33.5	22	*Adv. Funct. Mater.* **2025**, *35*, 2412044
(*S*)-S-AX-BN	-3.2×10^{-3}	-	-	
(*R*)-SO_2-AX-BN	2.2×10^{-3}	31.5	21	
(*S*)-SO_2-AX-BN	-2.1×10^{-3}	-	-	
(*P*)-BN-TP-ICz	6.49×10^{-4}	32.0	38	*Chem. Sci.* **2024**, *15*, 15170-15177
(*M*)-BN-TP-ICz	-7.74×10^{-4}	-	-	
(*R*)-BNP-o-CzPI	1.44×10^{-3}	7.2	50	*Chem. Eng. J.* **2024**, *499,* 156195
(*S*)-BNP-o-CzPI	-3.1×10^{-3}	6.9	50	
$(F8BT)_{0.9}$-$(R\text{-}5011)_{0.1}$-$(DBN\text{-}ICZ)_{0.005}$	0.16	4.6	39	*Adv. Mater.* **2024**, *36*, 2406550.
$(F8BT)_{0.9}$-$(S\text{-}5011)_{0.1}$-$(DBN\text{-}ICZ)_{0.005}$	-0.11	4.4	39	
R-PBN	5×10^{-2}	8.2	36	*Angew. Chem. Int. Ed.* **2024**, *63*, e202412283
S-PBN	-7×10^{-2}	9.8	37	

D-(*R*)-NBNPO	1.46×10^{-3}	28.3	29	*Mater. Horiz.* **2024**, *11*, 4722-4729
D-(*S*)-NBNPO	-1.40×10^{-3}	-	-	
D-(*R*)-NBOPO	7.02×10^{-4}	16.4	31	
D-(*S*)-NBOPO	-7.80×10^{-4}	-	-	
(*R*)-DtCzB-OBN	3.4×10^{-4}	-	-	*Adv. Opt. Mater.* **2024**, *12*, 2400685
(*S*)-DtCzB-OBN	-3.1×10^{-4}	30.0	22	
(*R*)-DtCzB-BN	7.9×10^{-4}	-	-	
(*S*)-DtCzB-BN	-8.1×10^{-4}	33.9	22	
R/*S*-D1	0.88×10^{-3}	14.9	43	*Adv. Mater.* **2024**, *36*, 2311857
R/*S* -D4	1×10^{-3}	24.1	27	
R/*S* -D5	3.6×10^{-3}	17.9	28	
R/*S* -D6	2×10^{-3}	25.4	40	
P-BN[9]H	-6.2×10^{-3}	35.4	48	*Angew. Chem. Int. Ed.* **2024**, *63*, e202401835
M-BN[9]H	4.9×10^{-3}	35.5	48	
M-*o*[B-N]$_2$N$_2$	$+7.7 \times 10^{-4}$	25.1	33	*Sci. China Chem.* **2023**, *66,* 2612
P-*o*[B-N]$_2$N$_2$	-6.7×10^{-4}	25.1	33	
(*P*)-BN-Py	-4.37×10^{-4}	30.6	37	*Adv. Mater.* **2023**, *35*, 2305125
(*M*)-BN-Py	$+4.35 \times 10^{-4}$	29.2	37	
(*M*)-DB-O	$+2.2 \times 10^{-3}$	27.5	24	*Adv. Mater.* **2024**, *36*, 2308314
(*P*)-DB-O	-2.2×10^{-3}	26.2	24	
(*M*)-DB-S	$+2.6 \times 10^{-3}$	29.3	24	
(*P*)-DB-S	-2.6×10^{-3}	28.9	24	
M,M-RBNN	$+1.91 \times 10^{-3}$	36.6	48	*Adv. Mater.* **2024**, *36*, 2307420
P,P-RBNN	-1.77×10^{-3}	34.4	48	
(*R*)-Czp-tBuCzB	$+1.54 \times 10^{-3}$	32.1	24	*Angew. Chem. Int. Ed.* **2023**, *62*, e202217045
(*S*)-Czp-tBuCzB	-1.48×10^{-3}	-	-	
(*R*)-Czp-POAB	$+1.30 \times 10^{-3}$	28.7	48	
(*S*)-Czp-POAB	-1.25×10^{-3}	-	-	
(*P*)-helicene-BN	$+1.2 \times 10^{-3}$	31.5	49	*CCS Chem.***2022**, *4,* 3463
(*M*)-helicene-BN	-2.2×10^{-3}	30.7	50	
R-DOBN	-9×10^{-4}	23.9	38	*Adv. Mater.* **2022**, *34,* 2204253
S-DOBN	$+9 \times 10^{-4}$	23.7	38	
R-DOBNT	-1×10^{-3}	25.6	35	
S-DOBNT	$+9 \times 10^{-4}$	24.0	35	
(*R*)-BN-MeIAc	$+2.7 \times 10^{-4}$	37.2	33	*Angew. Chem. Int. Ed.* **2022**, *61,* e202202227
(*S*)-BN-MeIAc	-2.8×10^{-4}	36.1	33	
R-CzOBN : POT2T : BN1	2.8×10^{-3}	33.2	42	*Adv. Mater.* **2022**, *34,*

S-CzOBN : POT2T:BN1	-2.8×10^{-3}	32.9	42	2109147
(+)-BN4	$+4.6 \times 10^{-4}$	20.6	49	*Adv. Mater.* **2022**, *34,* 2105080
(-)-BN4	-7.6×10^{-4}	19.0	49	
(+)-BN5	$+1.43 \times 10^{-3}$	22.0	48	
(-)-BN5	-1.27×10^{-3}	26.5	48	
(*R*)-OBN-2CN-BN	$+1.43 \times 10^{-3}$	29.4	30	*Adv. Mater.* **2021**, *33,* 2100652
(*S*)-OBN-2CN-BN	-1.27×10^{-3}	-	33	
(*R*)-OBN-4CN-BN	$+4.60 \times 10^{-4}$	24.5	33	
(*S*)-OBN-4CN-BN	-4.76×10^{-4}	-	34	

11. NMR spectra and HR-MS of Compounds.

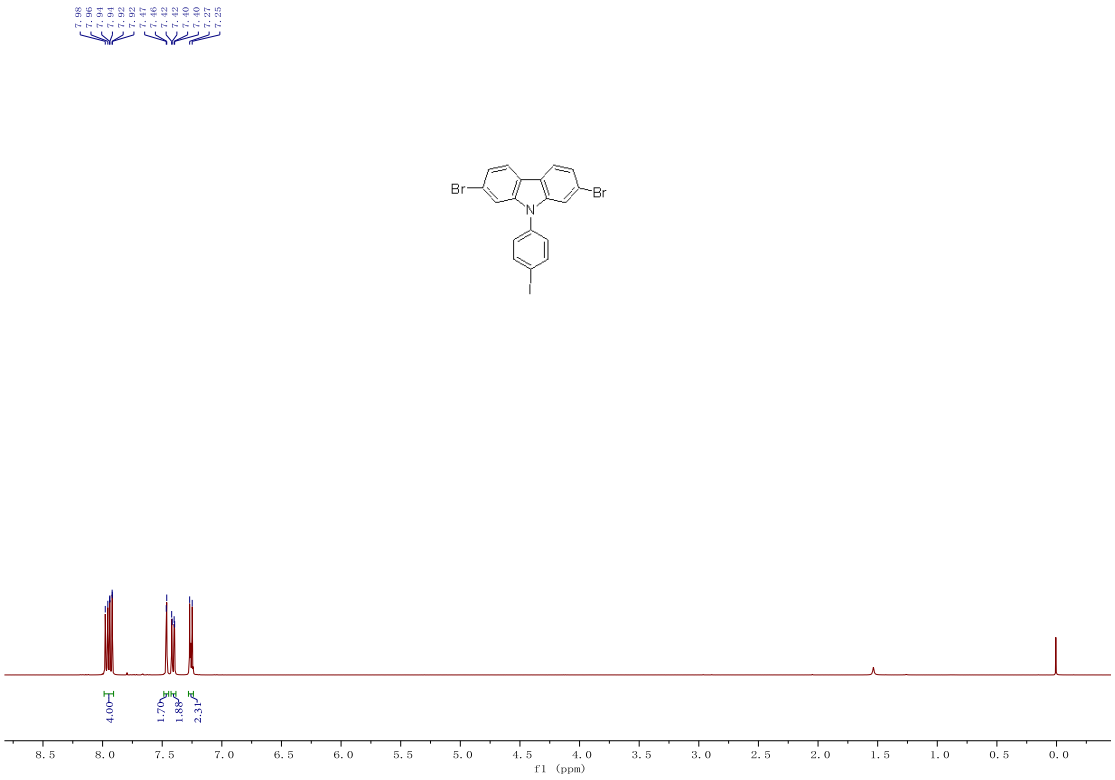

Fig. S14. ^{1}H NMR spectrum of 1 (400 MHz, $CDCl_3$).

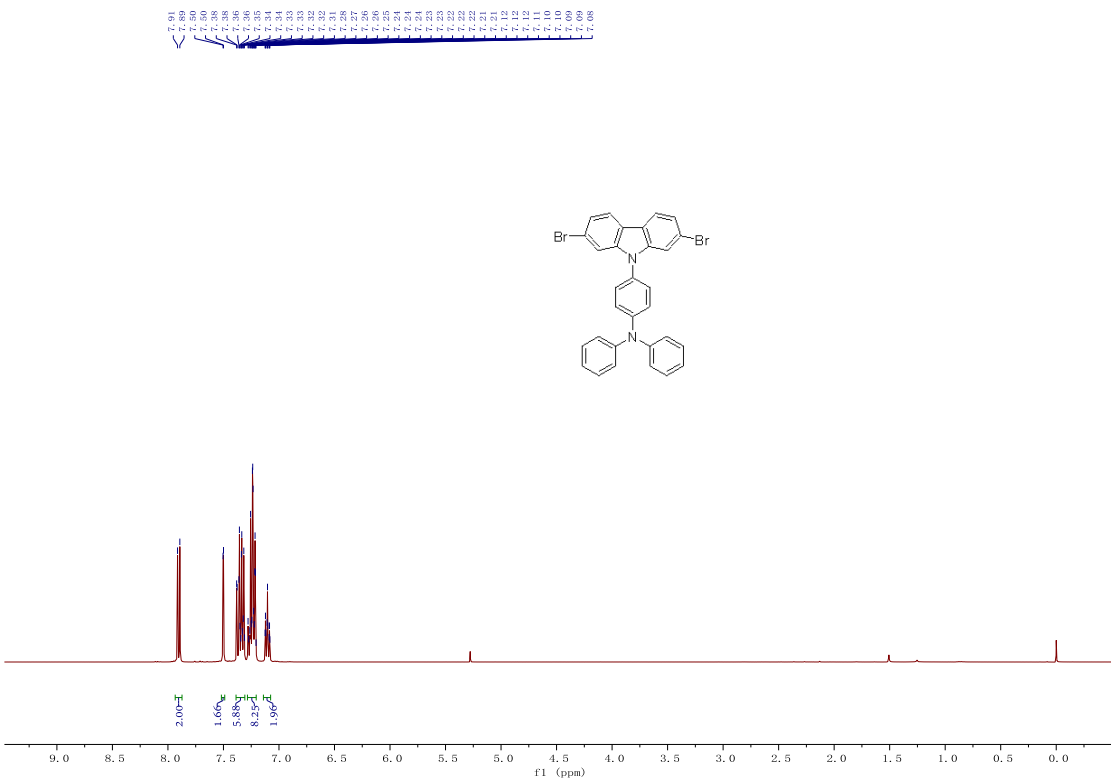

Fig. S15. ^{1}H NMR spectrum of 2 (400 MHz, $CDCl_3$).

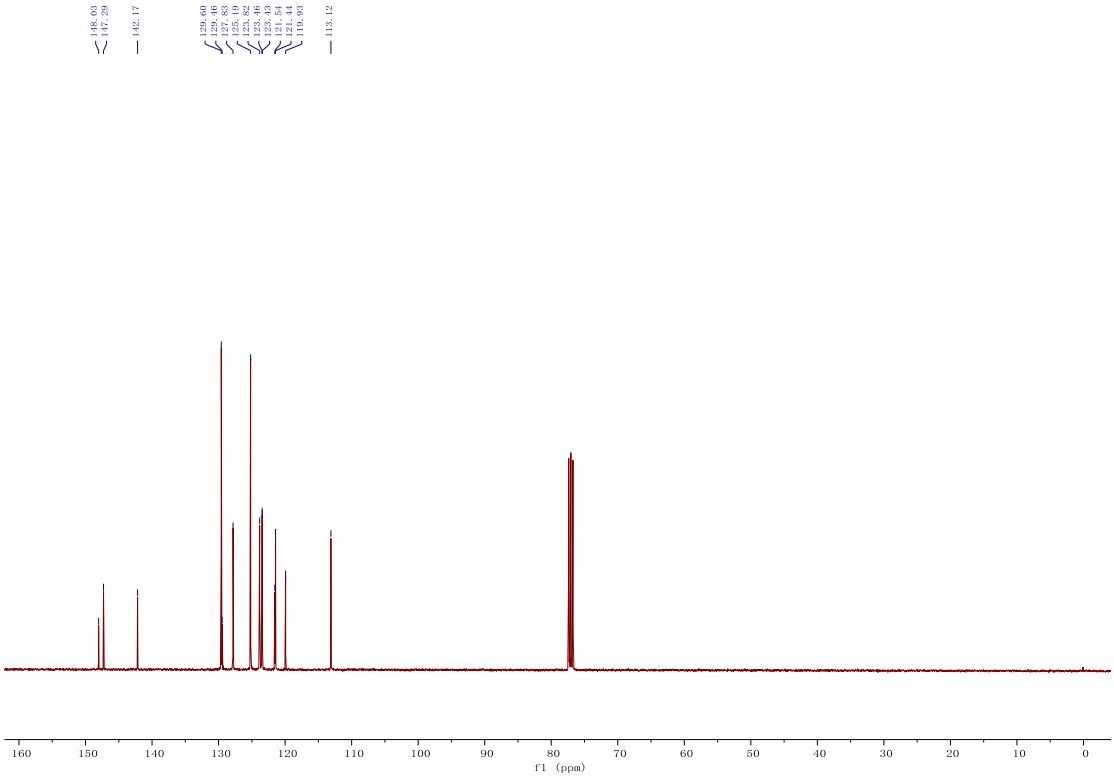

Fig. S16. ^{13}C NMR spectrum of 2 (101 MHz, $CDCl_3$).

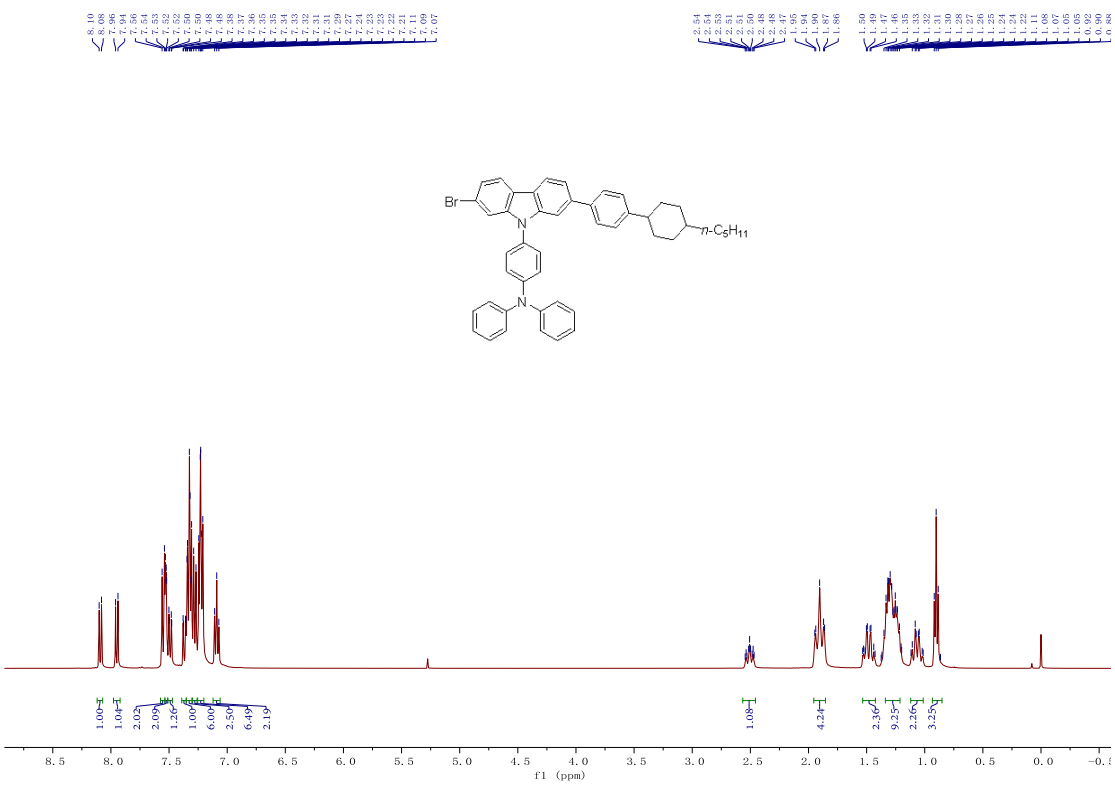

Fig. S17. ^{1}H NMR spectrum of 3 (400 MHz, $CDCl_3$).

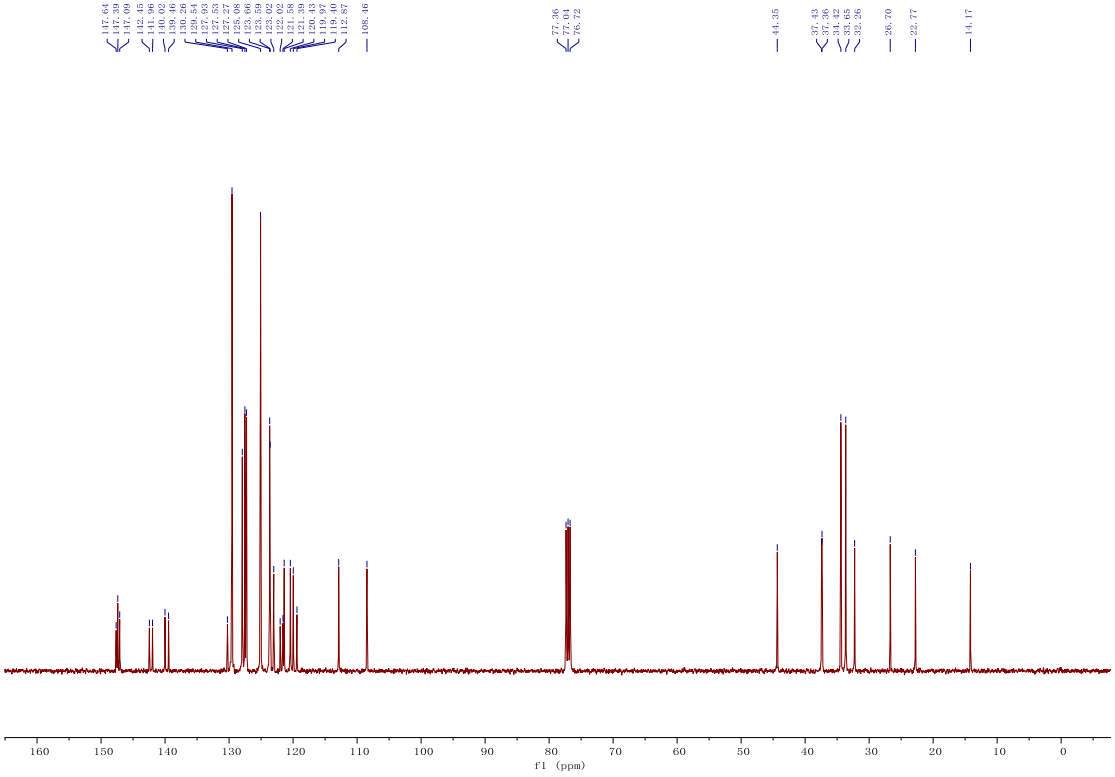

Fig. S18. ^{13}C NMR spectrum of 3 (101 MHz, $CDCl_3$).

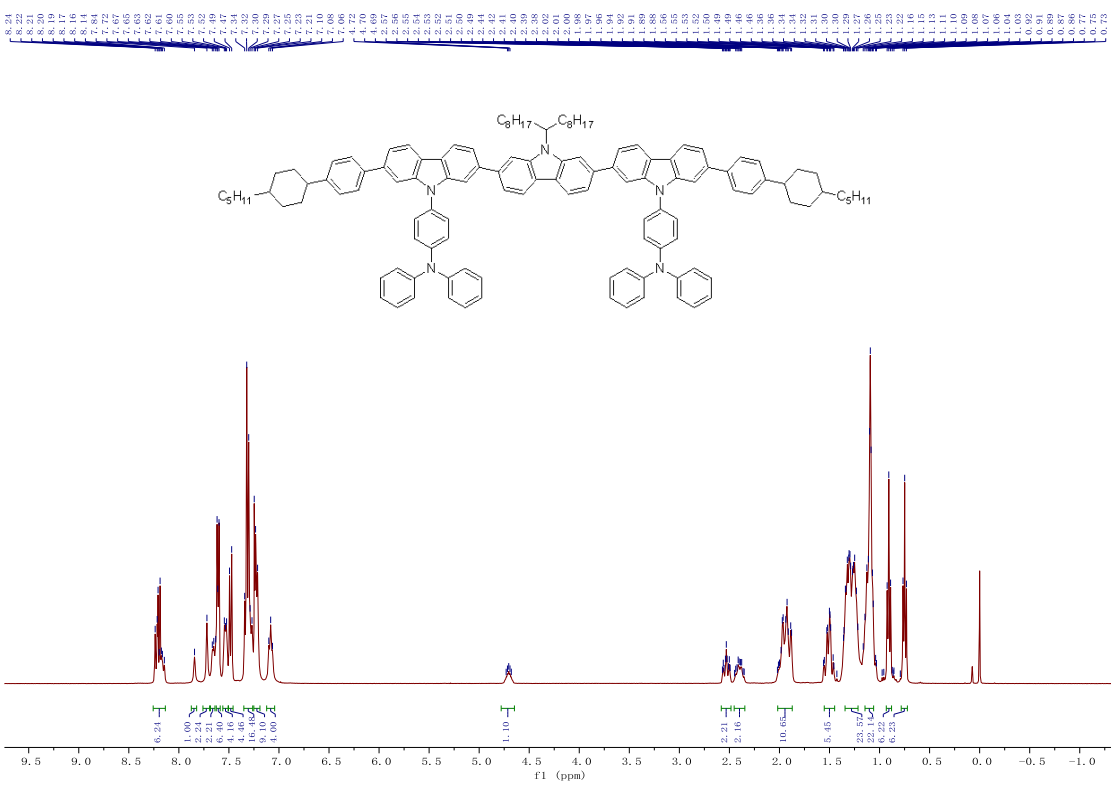

Fig. S19. ^{1}H NMR spectrum of CzTPA (400 MHz, $CDCl_3$).

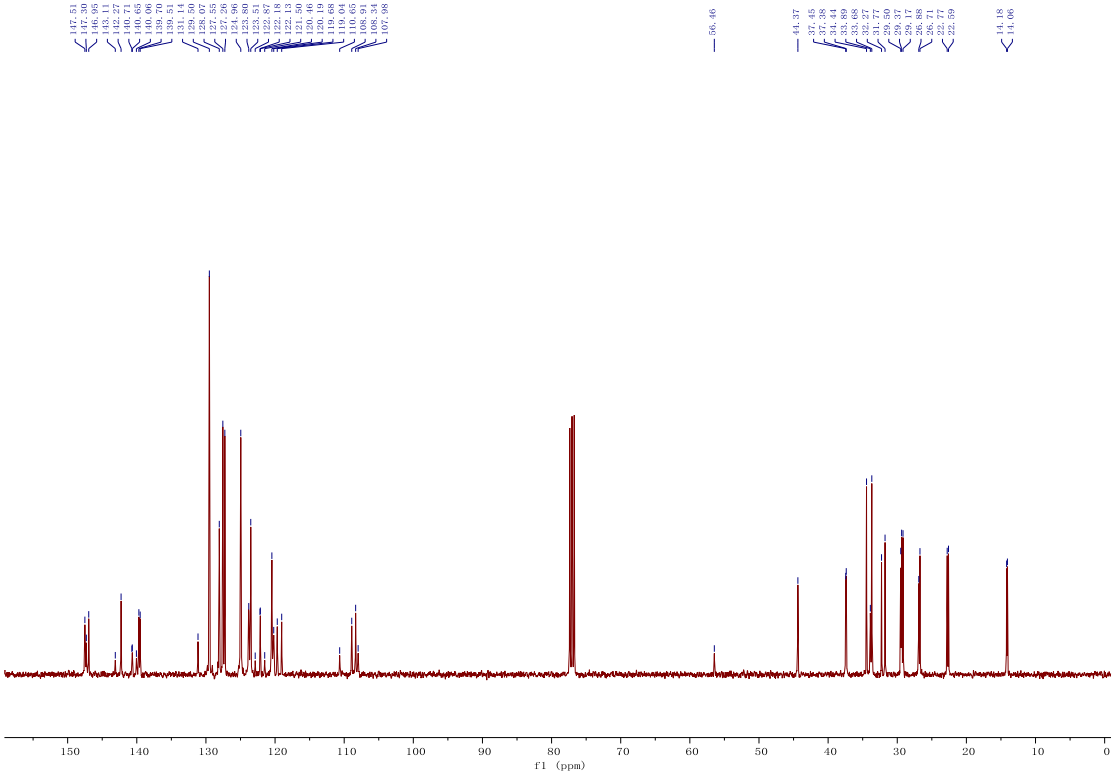

Fig. S20. ^{13}C NMR spectrum of CzTPA (101 MHz, $CDCl_3$).

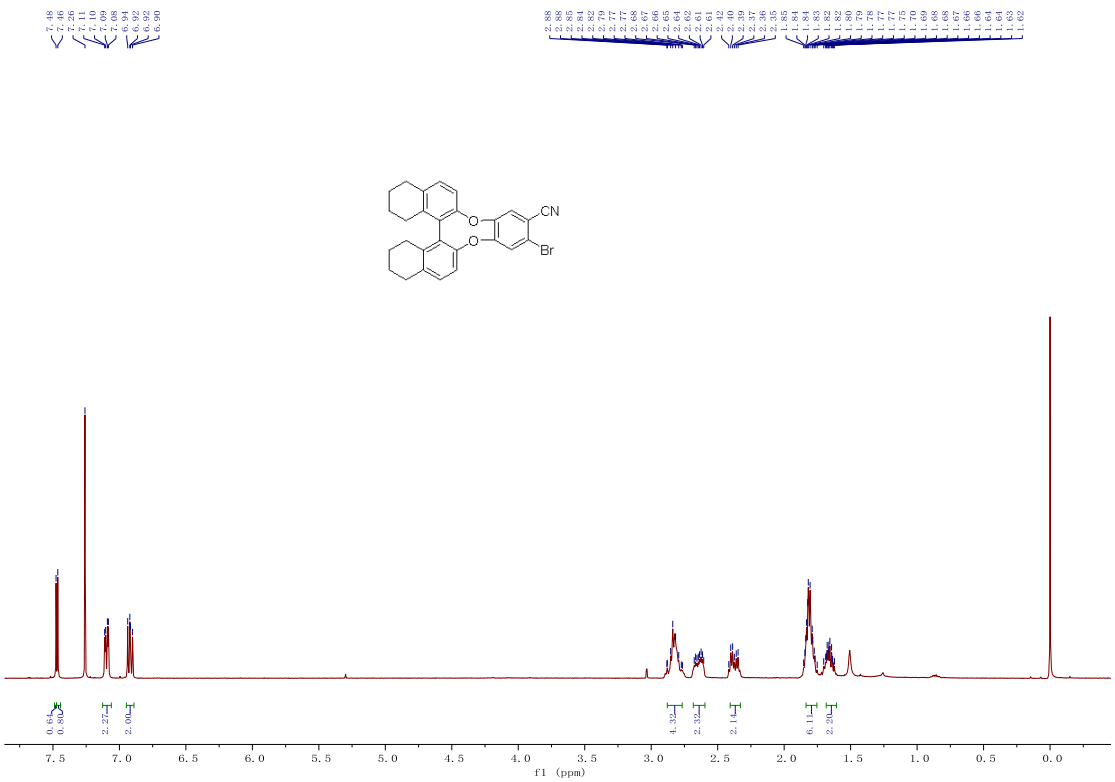

Fig. S21. ^{1}H NMR spectrum of *R*/*S*-4 (400 MHz, $CDCl_3$).

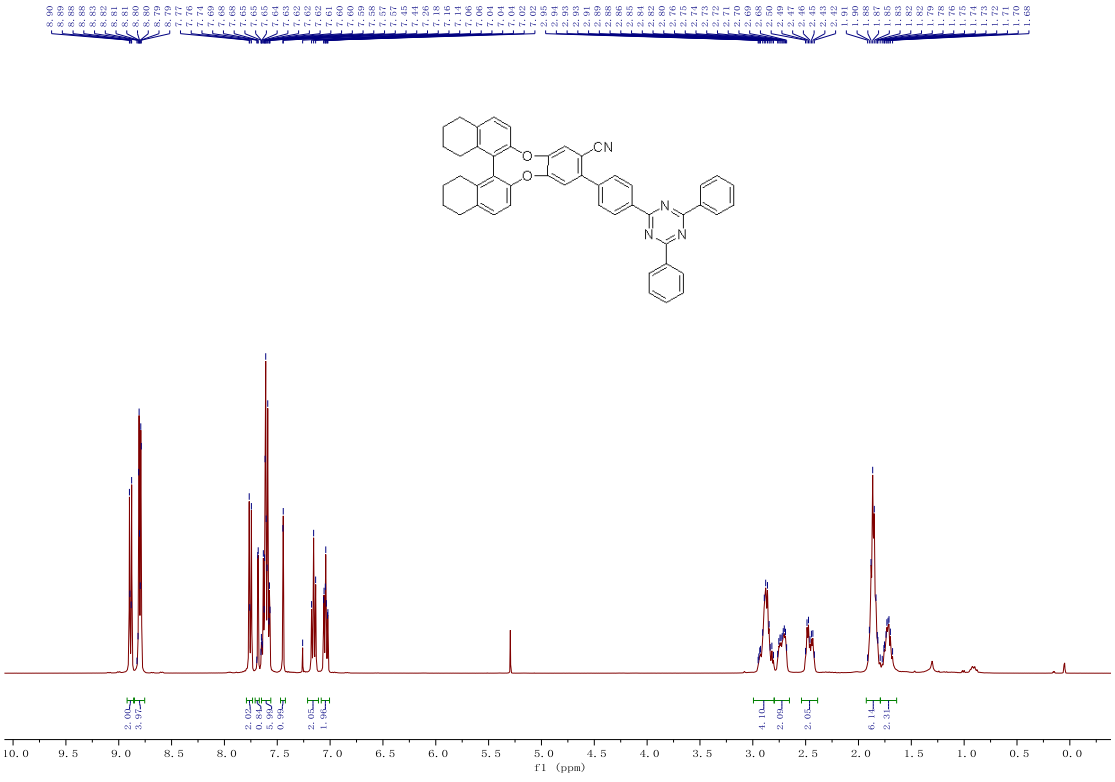

Fig. S22. ^{1}H NMR spectrum of *R*/*S*-TRZ (400 MHz, $CDCl_3$).

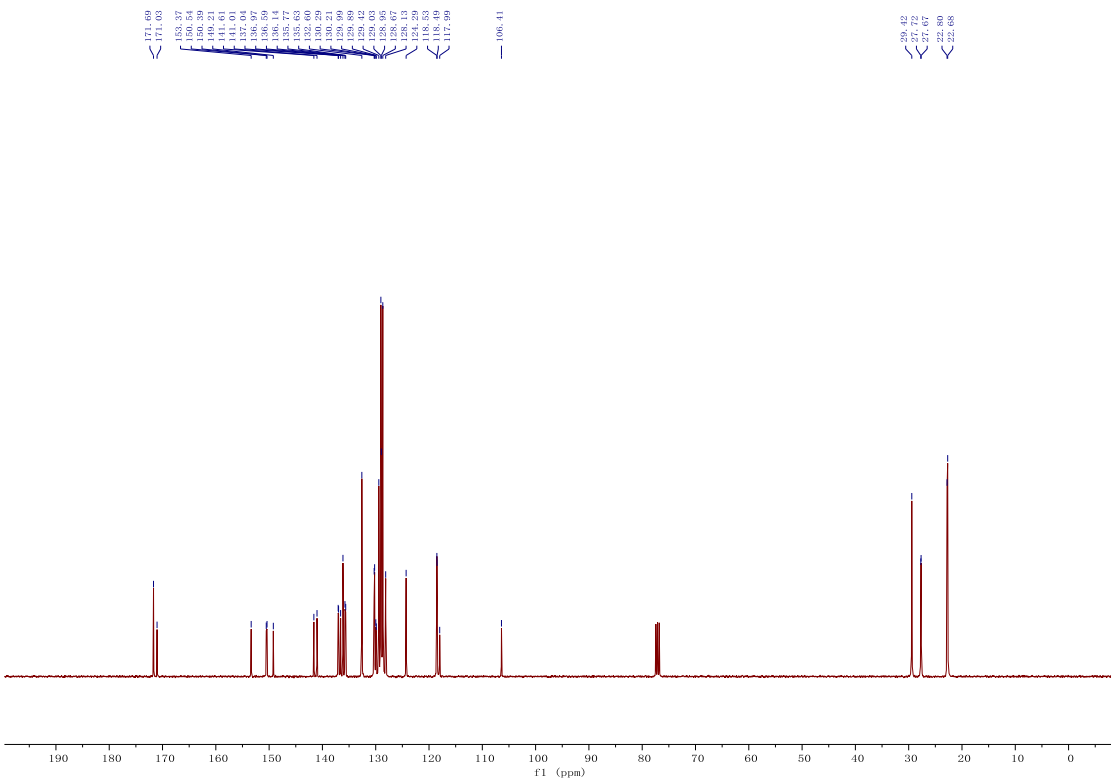

Fig. S23. ^{13}C NMR spectrum of *R*/*S*-TRZ (101 MHz, $CDCl_3$).

12. References

S1 T. Wang, X. Yin, X. Cao and C. Yang, *Angew. Chem. Int. Ed.*, 2023, **62**, e202301988.

S2 M. J. Frisch, G. W. Trucks, H. B. Schlegel, G. E. Scuseria, M. A. Robb, J. R. Cheeseman, G. Scalmani, V. Barone, G. A. Petersson, H. Nakatsuji, X. Li, M. Caricato, A. Marenich, J. Bloino, B. G. Janesko, R. Gomperts, B. Mennucci, H. P. Hratchian, J. V. Ortiz, A. F. Izmaylov, J. L. Sonnenberg, D. Williams-Young, F. Ding, F. Lipparini, F. Egidi, J. Goings, B. Peng, A. Petrone, T. Henderson, D. Ranasinghe, V. G. Zakrzewski, J. Gao, N. Rega, G. Zheng, W. Liang, M. Hada, M. Ehara, K. Toyota, R. Fukuda, J. Hasegawa, M. Ishida, T. Nakajima, Y. Honda, O. Kitao, H. Nakai, T. Vreven, K. Throssell, J. A. Montgomery, Jr., J. E. Peralta, F. Ogliaro, M. Bearpark, J. J. Heyd, E. Brothers, K. N. Kudin, V. N. Staroverov, T. Keith, R. Kobayashi, J. Normand, K. Raghavachari, A. Rendell, J. C. Burant, S. S. Iyengar, J. Tomasi, M. Cossi, J. M. Millam, M. Klene, C. Adamo, R. Cammi, J. W. Ochterski, R. L. Martin, K. Morokuma, O. Farkas, J. B. Foresman, and D. J. Fox, *Gaussian 09, Revision A.02*, Gaussian, Inc., Wallingford CT,: 2016.

S3 P. J. Stephens, F. J. Devlin, C. F. Chabalowski and M. J. Frisch, *J. Phys. Chem.*, 1994, **98**, 11623-11627.

S4 Y. Xie, X. Wang, Q. Chen, S. Liu, Y. Yun, Y. Liu, C. Chen, J. Wang, Y. Cao, F. Wang, T. Qin and W. Huang, *Macromolecules*, 2019, **52**, 4757-4764.

S5 Y. Xu, Q. Wang, X. Cai, C. Li and Y. Wang, *Adv. Mater.*, 2021, **33**, 2100652.